Earthq Sci (2016) 29(2):105–115
DOI 10.1007/s11589-016-0146-3

RESEARCH PAPER

# Crustal stress field in Yunnan: implication for crust-mantle coupling

**Zhigang Xu · Zhouchuan Huang · Liangshu Wang · Mingjie Xu · Zhifeng Ding · Pan Wang · Ning Mi · Dayong Yu · Hua Li**

Received: 17 November 2015 / Accepted: 17 February 2016 / Published online: 1 April 2016


**Abstract** We applied the gCAP algorithm to determine 239 focal mechanism solutions ($3.0 \leq M_W \leq 6.0$) with records of dense ChinArray stations deployed in Yunnan, and then inverted 686 focal mechanisms (including 447 previous results) for the regional crustal stress field with a damped linear inversion. The results indicate dominantly strike-slip environment in Yunnan as both the maximum ($\sigma_1$) and minimum ($\sigma_3$) principal stress axes are sub-horizontal. We further calculated the horizontal stress orientations (i.e., maximum and minimum horizontal compressive stress axes: $S_H$ and $S_h$, respectively) accordingly and found an abrupt change near $\sim$26°N. To the north, $S_H$ aligns NW-SE to nearly E-W while $S_h$ aligns nearly N-S. In contrast, to the south, both $S_H$ and $S_h$ rotate laterally and show dominantly fan-shaped patterns. The minimum horizontal stress (i.e., maximum strain axis) $S_h$ rotates from NW-SE to the west of Tengchong volcano gradually to nearly E-W in west Yunnan, and further to NE-SW in the South China block in the east. The crustal strain field is consistent with the upper mantle strain field indicated by shear-wave splitting observations in Yunnan but not in other regions. Therefore, the crust and upper mantle in Yunnan are coupled and suffering vertically coherent pure-shear deformation in the lithosphere.

**Keywords** Tibet · Yunnan · Focal mechanism solution · Stress field · Crust-mantle coupling

## 1 Introduction

The tectonic evolution of the Tibetan plateau (Fig. 1a), especially its rapid uplift, has always been the focus in geosciences. Different mechanisms have been proposed among which the lateral lithospheric extrusion (e.g., Tapponnier et al. 1982, 2001), thickening Asian crust (England and Houseman 1989), and ductile mid-lower crustal flow (e.g., Royden et al. 1997, 2008) are three most popular candidates. The structures and dynamics in SE Tibet are essentially important for understanding the tectonic evolution of the plateau. However, there is ongoing debates on whether the crust and upper mantle are coupled or not beneath Yunnan SE to Tibet on the basis of the comparison between the crustal strain field inferred from GPS observations and the upper-mantle strain field inferred from teleseismic shear-wave (i.e., SKS, SKKS, and PKS) splitting analysis (e.g., Flesch et al. 2005; Wang et al. 2008; Huang et al. 2015a).

Yunnan is located in the southern part of the North-South seismic zone that is characterized as high seismicity and heavy seismic hazards (Fig. 1b). The focal mechanism solutions of small-to-moderate earthquakes are important indicators of the stress field near the source, i.e., generally in the crust under continents. Thus inverting for the focal

**Electronic supplementary material** The online version of this article (doi:10.1007/s11589-016-0146-3) contains supplementary material, which is available to authorized users.

Z. Xu · Z. Huang (✉) · L. Wang · M. Xu · P. Wang · N. Mi · D. Yu · H. Li
State Key Laboratory for Mineral Deposits Research, School of Earth Sciences and Engineering, Nanjing University, Nanjing 210046, China
e-mail: ihuangz@nju.edu.cn

Z. Xu · Z. Huang · L. Wang · M. Xu · P. Wang · N. Mi · D. Yu · H. Li
Institute of Geophysics and Geodynamics, Nanjing University, Nanjing 210046, China

Z. Ding
Institute of Geophysics, China Earthquake Administration, Beijing 100081, China

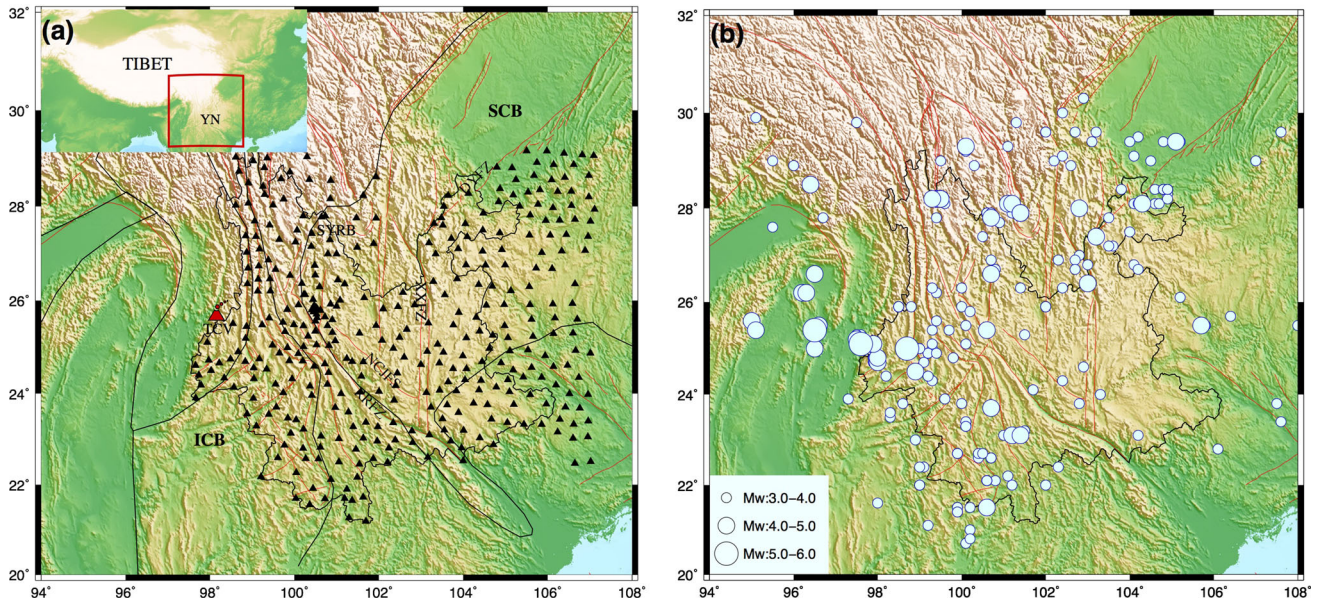


**Fig. 1** Tectonics in SE Tibet. **a** *Black triangles* show 343 temporary station in Yunnan (YN) deployed by the ChinArray project. *Black* and *red curves* denote major tectonic boundaries (Ren 1999) and active faults, respectively. The *red triangle* denotes the Tengchong volcano (TCV). The abbreviations are: *SCB* Sichuan basin, *SYRB* Sichuan-Yunnan rhombic block, *ICB* Indochina Block, *RRFZ* Red-River fault zone, *XXFZ* Xianshui-Xiaojiang fault zone, *DYFZ* Deyuzuo-Yinmahu fault zone; *NCJFZ* Nanhua-Chuxiong-Jianshui fault zone. **b** *Circles* denote 327 local events recorded by the ChinArray stations during August 2011 to December 2013. The sizes of the *circles* denote the magnitudes of the events with the scale shown in the *bottom-left inset*

mechanisms in Yunnan may help to understand the stress/strain field in the crust, which is important for discussing the crust-mantle coupling/decoupling model in SE Tibet. Many previous researchers determined the earthquake focal mechanisms there with such an approach and studied the stress field in different blocks as well as the influence of the active faults (e.g., Xu et al. 1987, 2010; Xie et al. 1993; Qian et al. 2011; Cui et al. 2006; Ma et al. 2008; Luo et al. 2014). Zhao et al. (2013) further derived the regional stress field in Yunnan through a damped linear inversion (Hardebeck and Michael 2006) using the focal mechanisms obtained from records of the permanent stations and the gCMT catalogue. They found that Yunnan is under a strike-slip faulting regime dominated by horizontal maximum and minimum principle stresses and that the orientation of the maximum principle stress axis clearly follows the surface horizontal velocity field from GPS observations (Zhao et al. 2013).

In this study, we first obtained the focal mechanism solutions of 239 events $(3.0 \leq M_W \leq 6.0)$ recorded by dense ChinArray stations deployed in Yunnan with the gCAP algorithm. The dense stations allows us to determine the focal mechanisms for earthquakes of magnitude down to $M_W$ 3.0 (compared with $M_W \geq 3.4$ with permanent stations in previous studies), which provides better space coverage. We then inverted the improved dataset for the regional stress field with a damped linear inversion (Hardebeck and Michael 2006) and compared it with the upper-mantle strain field indicated by shear-wave splitting measurements. The results suggest coupled crust and mantle in Yunnan, which improves our understanding of the tectonic evolution of the Tibetan Plateau.

## 2 Focal mechanism solutions

The waveform used in this study is recorded by 343 portable stations (Fig. 1a) of the ChinArray project deployed in SE Tibet (mostly in Yunnan province) during August 2011 to December 2013. Most of the stations were equipped with a Guralp CMG-3EPC three-component broadband seismometer and a Reftek-130 digitizer. The sampling rates are 100 samples per second. We collected a total of 372 local events with $3.0 \leq M_W \leq 6.0$ occurred in this region.

In this study, we used the generalized Cut-and-Paste (gCAP) method (Zhao and Helmberger 1994; Zhu and Helmberger 1996; Zhu and Ben-Zion 2013) to determine the seismic moment tensors of the local events. The method selects five phase windows (i.e., two P-wave windows on the vertical and radial components and three S-wave windows on all three components) for

3-component seismograms recorded at each station. The synthetic waveforms were modeled with the F-K algorithm (Aki and Richards 2002; Zhu and Rivera 2002). The 1D velocity model (Fig. 2a) was derived from the layered model from seismic exploring (e.g., Wang et al. 2003). The fit between synthetic and observational seismograms is calculated separately for the short-period P-wave and long-period S-wave windows. Different time-shifts and weights were used for P and S wave windows to reduce to uncertainties induced by 1D velocity model and to avoid the dominance of surface wave, respectively. The grid-search algorithm is applied to search for the optimal moment tensors that minimize the misfit between the synthetic and observational waveforms.

Figure 2 shows the 1D velocity model and an example of gCAP solution for an $M_W$ 4.1 event occurring on 16 October 2011. We only used the records at stations with epicentral distances smaller than 400 km. Figure 2c shows both the synthetic and observational waveforms. The correlation coefficient is generally greater than 0.7 for P-wave windows (80 %) and greater than 0.8 for S-wave windows (90 %), which indicates that the result is reliable. Finally, we obtained 239 robust focal mechanism solutions from the 372 events analyzed (Table S1). Most of the event occurred at depths of <20 km and have the magnitudes of $M_W$ 3.0–4.0 (Fig. 3a). The general pattern of the focal mechanisms (Fig. 3a) is similar to previous studies (Fig. 3b; Tables S2–S4) (e.g., Xu et al. 2010; Zhao et al. 2013; Luo et al. 2014). Most of the earthquakes are strike-slip events, which is consistent with the dominant strike-slip regime in Yunnan due to the India-Asian collision (e.g., Tapponnier et al. 1982, 2001). However, we also found some normal and thrust type events in south Yunnan (i.e., Indochina Block) (Fig. 3a) that were not visible in previous studies with permanent stations (Fig. 3b). It may indicate that the occurring of smaller events ($\sim M_W$ 3.0) is affected significantly by local structures in smaller scale (e.g., Scholz 2002; Huang et al. 2011b). In contrast, for larger events ($M_W \geq 3.4$), the regional stress field is more important.

The stress field inferred from the focal mechanisms shows important transition from north to south at 26°–28°N (Fig. 4). To the north, the *P*-axis mainly aligns E-W while the T-axis is nearly N-S. It reflects the E-W compression regime because the eastern expansion of the Tibetan Plateau is blocked by the stable Sichuan basin (i.e., Yangtze Craton). To the south, the dominant *P* and *T* axes are N-S and E-W, respectively. However, both *P* and *T* axes show important rotations. The *P*-axis rotates anticlockwise from NE-SW in the west gradually to NW-SE in the east while *T*-axis rotates anticlockwise from NW-SE in the west to NE-SW in the east.

## 3 Stress field inversion

The earthquakes occurred on a preexisting weak zone or fault and the stress directions inferred from individual focal mechanisms may show considerable lateral variations (e.g., Scholz 2002). Instead, the regional stress field can be estimated from a group of events in a limited area (e.g., Gephart and Forsyth 1984; Michael 1987; Huang et al. 2011a). In this study, we used the MSATSI toolbox (Martinez-Garzon et al. 2014) to apply the damped regional-scale linear inversion (Hardebeck and Michael 2006; Michael 1987) and inverted the 686 focal mechanism solutions (239 in this study and 447 in previous studies) for the uniform stress field in Yunnan. The method divides the study region into many subareas and simultaneously invert for stress field (Michael 1987) in all subareas while minimizing the difference in stress between adjacent subareas. It is a least-squares solution of the equation:

$$\left(\boldsymbol{G}^{\mathrm{T}}\boldsymbol{G} + e^2\boldsymbol{D}^{\mathrm{T}}\boldsymbol{D}\right)\boldsymbol{m} = \boldsymbol{G}^{\mathrm{T}}\boldsymbol{d},$$

where $\boldsymbol{m}$ is the model vector containing the stress tensor elements at the grid points, $\boldsymbol{d}$ is the data vector including the slip vector components of earthquakes at the corresponding grid points, and $G$ is the data kernel matrix involving the normal vector components of all the fault planes. The matrix $\boldsymbol{D}$ is the damping matrix formed by blocks of zeros, the identity matrix $\boldsymbol{I}$ and its opposite $-\boldsymbol{I}$, which is used to minimize the difference in stress between adjacent subareas. $e$ is the damping parameter to adjust the strength of damping. The damped inversion may well resolve the general pattern of the stress field in a region (Hardebeck and Michael 2006) while removing some local features due to geological activities such as active faults (e.g., Hardebeck and Hauksson 2001; Huang et al. 2011b).

We first inverted for the smoothed stress field in Yunnan with the 239 focal mechanism solutions obtained in this study (Fig. 5a) and then with all of the 686 solutions by combining previous results (Fig. 5b). Both results show dominantly similar patterns that suggest the crust beneath Yunnan is general under strike-slip environment (with both horizontal $\sigma_1$ and $\sigma_3$). The thrust regime is generally located to the west of the Sichuan basin where nearly E-W $\sigma_1$ is consistent with the eastward extrusion of the Tibet's materials. The normal regime is located in northwest Yunnan and $\sigma_3$ is sub-parallel to the active faults. Both $\sigma_1$ and $\sigma_3$ show important rotation from west to east (Fig. 5) that are comparable to the *P* and *T* axes of single focal mechanism solutions (Fig. 4), respectively. The first-order pattern is the same with previous studies that characterized the regional stress field in Yunnan, e.g., by focal mechanism solutions of many smaller events in a region (Xu et al. 1987), traditional stress field inversion with many focal

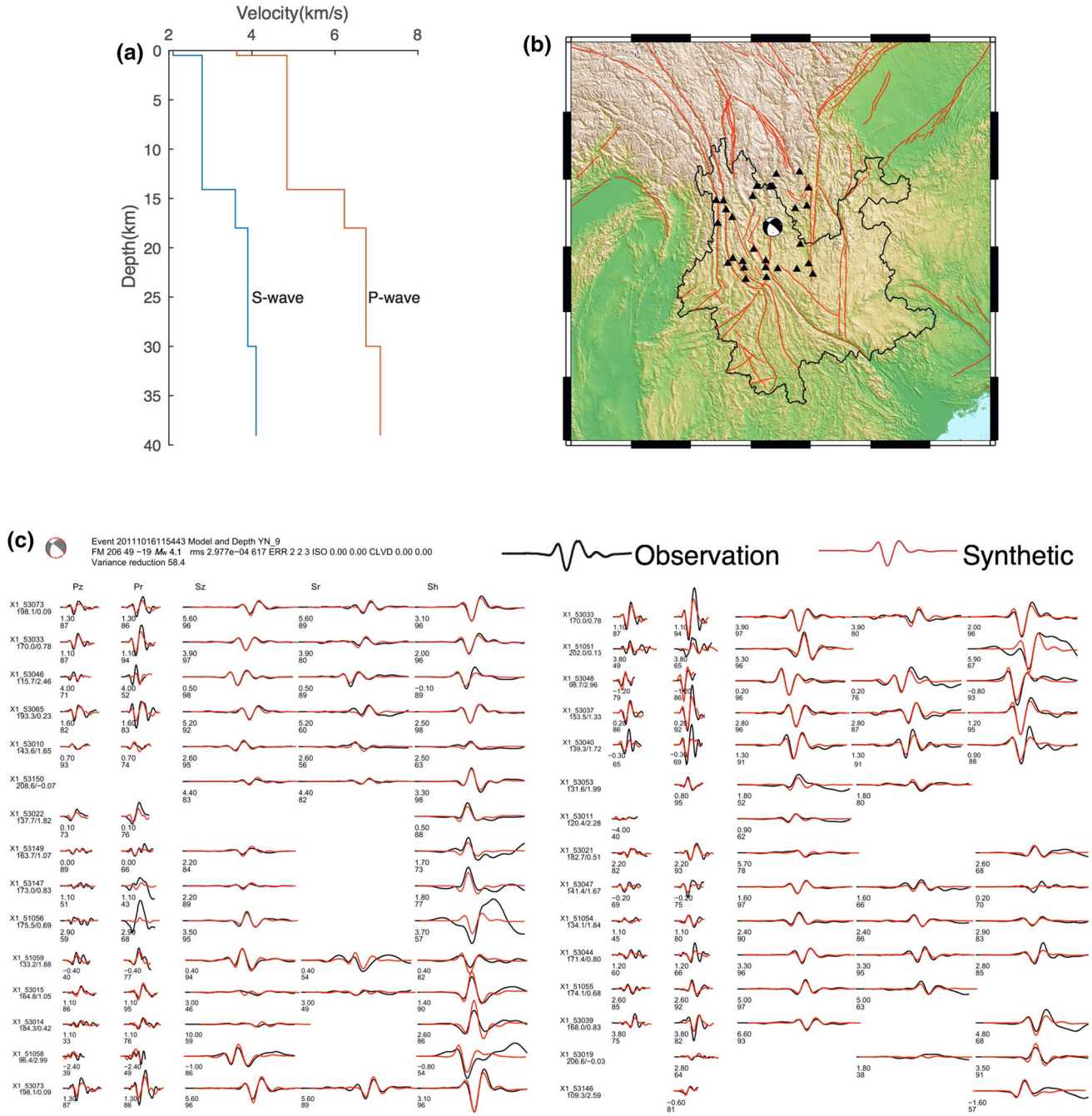


**Fig. 2** An example of the focal mechanism determination with the gCAP method for an earthquake occurring at 16 October 2011. **a** The 1D velocity model used in the study derived from Wang et al. (2003). **b** The locations of the event and corresponding stations used to determine the focal mechanisms. **c** Synthetic (*red*) and observational (*black*) seismograms at the stations marked in the *left*. The two numbers under each segment are the time shift in seconds between the synthetic and observational waveform (*upper*) and the waveform correlation coefficient (*lower*; 100 means best fit)

mechanisms in a region (e.g., Wan 2010), and damped stress inversion with focal mechanisms determined with permanent stations (Zhao et al. 2013). All these results show dominant abrupt change near 26°N–28°N, i.e., from E-W $\sigma_1$ and N-S $\sigma_3$ in the north to N-S $\sigma_1$ and E-W $\sigma_3$ in the south. The gradual transitions of both $\sigma_1$ (NE-SW → N-S → NW–SE from west to east) and $\sigma_3$ (NW–SE → E-W → NE-SW from west to east) in the south are also notable (Fig. 5). Note that adding more focal mechanism solution of smaller events recorded by the dense

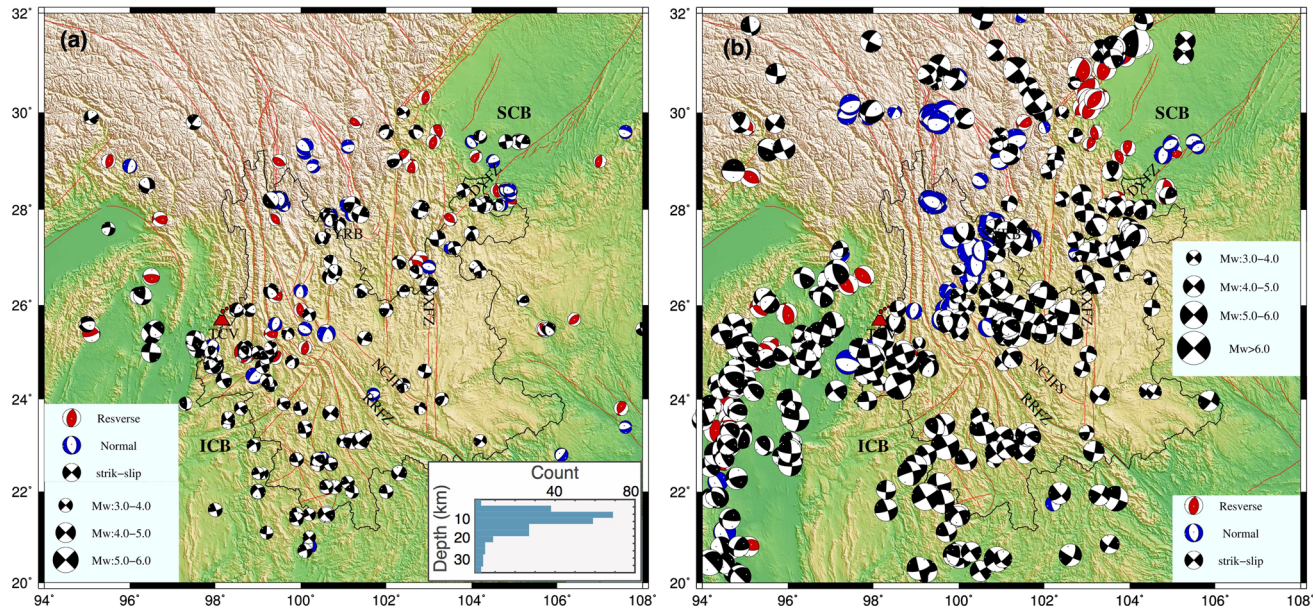


**Fig. 3** **a** 239 focal mechanism solutions obtained in the present study. The *red*, *blue*, and *black symbols* denote the reverse, normal, and strike-slip type events, respectively. The *sizes of the symbols* denote the magnitude of the events with the scale shown in the *bottom-left inset*. The statistics of the depths is showed in the *bottom-right inset*. **b** The same as (**a**) but for the 447 focal mechanism solutions collected from previous studies (Xu et al. 2010; Zhao et al. 2013; Luo et al. 2014) and the gCMT catalogue (1976–2015). For other labelings, see Fig. 1

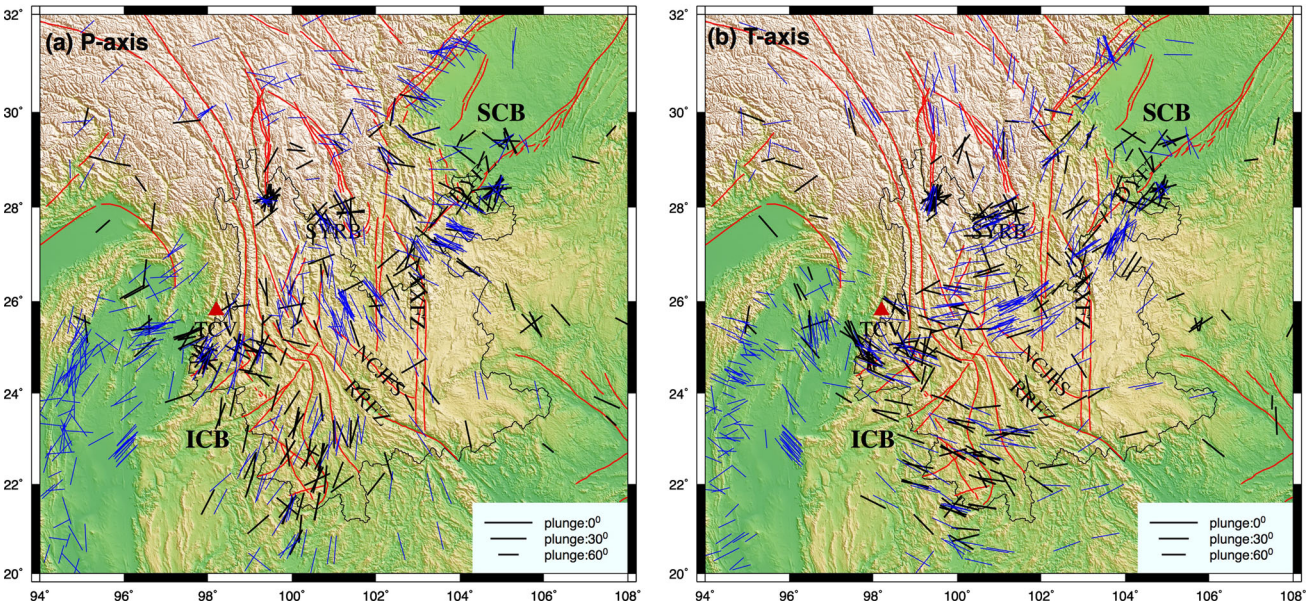


**Fig. 4** Orientations of **a** *P* and **b** *T* axes of the 686 focal mechanism solutions showed in Fig. 3. The *black and blue bars* denote the results of the 239 events determined in the present study and the 447 events of previous studies, respectively. The lengths of the show *bars* denote the plunges of the axes as shown in the *bottom-right inset*. For other labelings, see Fig. 1

ChinArray stations does not change the patterns of stress field in Yunnan compared with that of Zhao et al. (2013) (Figs. 4, 5, 6). The consistent result may due to the limited smaller events recorded in a short period in the dataset and, on the other hand, suggests robust and reliable stress inversion in Yunnan with the damped inversion method in this study.

In order to directly compare the present stress filed in the crust to that determined with GPS observations and mantle strain field inferred from shear-wave splitting

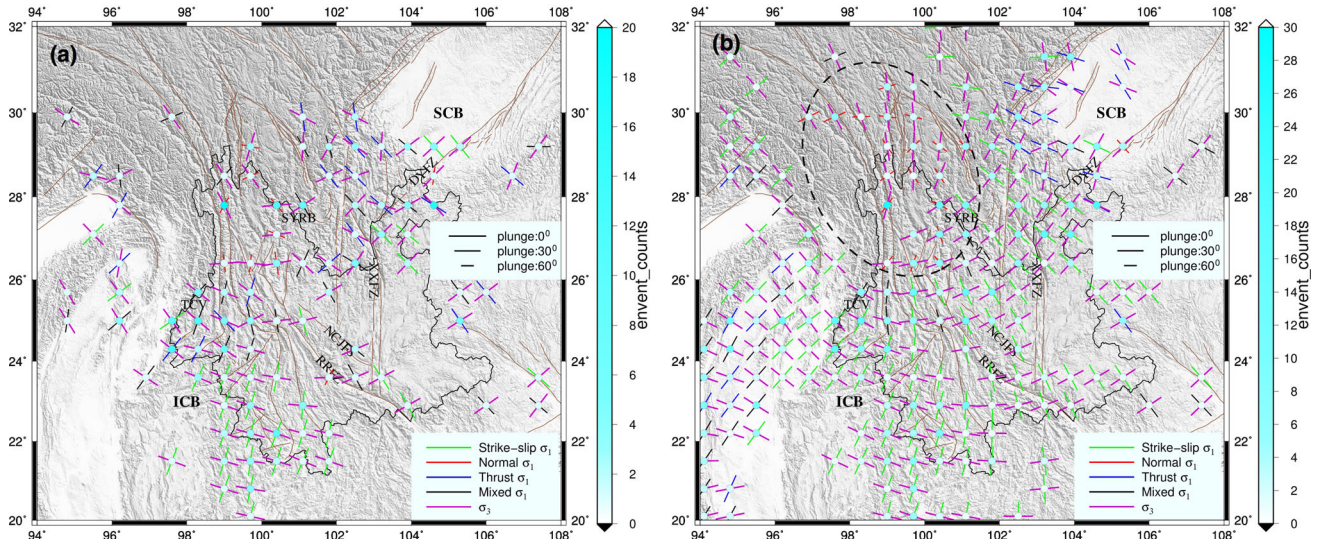


**Fig. 5** **a** Results of the stress field inversion from the 239 focal mechanism solutions shown in Fig. 3a on a 2D grid with uniform grid spacing of 0.7°. The *magenta bars* denote the orientations of the minimum principle stress axis $\sigma_3$ (i.e., tensional axis), while the *green*, *red*, *blue*, and *black bars* denote the orientations of the maximum principle stress axis $\sigma_1$ (i.e., compression) in the strike-slip, normal, thrust, and mixed faulting environments, respectively. The lengths of the show *bars* denote the plunges of the axes as scale shown in the *right inset*. The *colors of the circles* indicate the number of events at the corresponding grid node with the scale shown in the *right*. **b** Same as (**a**) but for the total 686 events by combining the 447 focal mechanism solutions collected from previous studies (Xu et al. 2010; Zhao et al. 2013; Luo et al. 2014) and the gCMT catalogue (1976–2015)

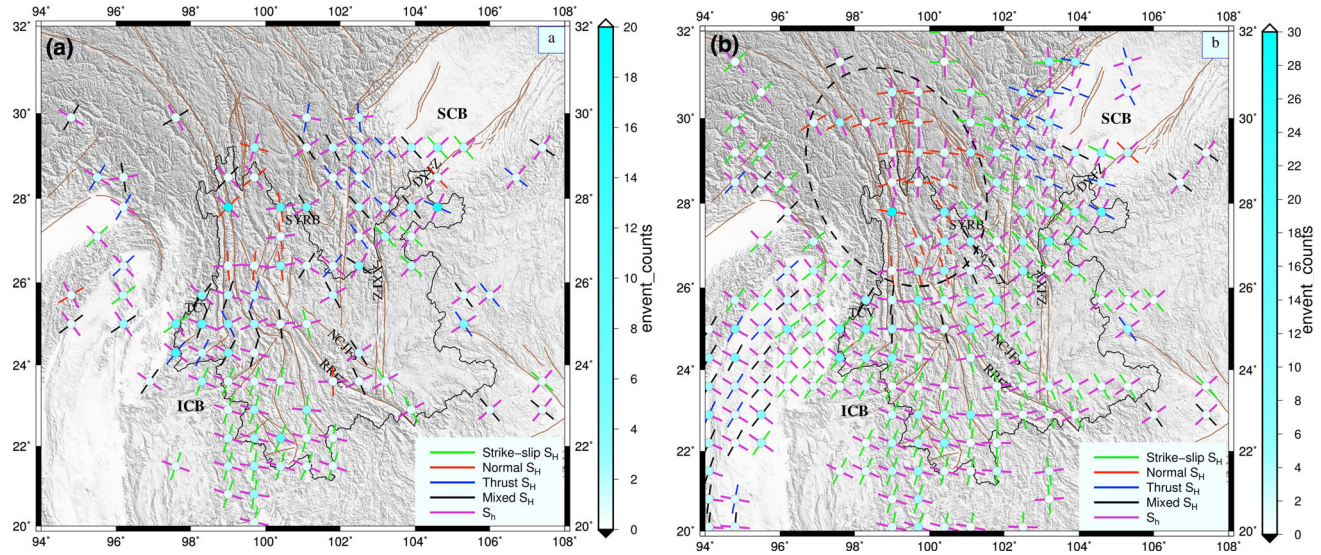


**Fig. 6** The maximum ($S_H$) and minimum ($S_h$) horizontal stress orientations calculated from the stress tensors shown in Fig. 5 (Lund and Townend 2007; Schimitt et al. 2012). The scales are shown in the *bottom-right inset*. For other labelings, see Figs. 1 and 5

measurements, we further calculate the horizontal stress orientations (i.e., maximum and minimal horizontal compressive stress: $S_H$ and $S_h$, respectively) from the stress tensors (Lund and Townend 2007; Schimitt et al. 2012) (Fig. 6). The results are similar to those revealed by *P* and *T* axes orientations (Fig. 4) and stress field inversions (Fig. 5), which clearly show the transition near 26°N–28°N (i.e., from dominantly E-W compression and N-S extension in the north to dominantly N-S compression and E-W extension in the south) as well as their rotation from west to east as mentioned above.

## 4 Discussion

As part of the North-South seismic zone with high seismicity and heavy seismic hazards, many previous studies determined the focal mechanisms of the small-to-moderate

events and discussed the crustal stress field in Yunnan and adjacent regions (e.g., Xu et al. 1987, 2010; Qian et al. 2011; Cui et al. 2006; Ma et al. 2008; Luo et al. 2014). In spite of the general pattern of the crustal stress field in Yunnan SE to Tibet from these earthquake focal mechanisms (Xu et al. 1987; Luo et al. 2014), these studies mainly revealed different stress orientations in different blocks separated by the active faults as well as the influence of these active faults (e.g., Xie et al. 1993; Qian et al. 2011; Cui et al. 2006; Xu et al. 2010). In this study, we applied the damped linear inversion (Hardebeck and Michael 2006) and inverted for the focal mechanism solutions for a smoothed regional crustal stress field in Yunnan (Figs. 5, 6). Unlike many previous studies, we focused on revealing the first-order pattern of stress/strain field in the crust under Yunnan. We tried to compare the tectonic deformation styles in the crust and upper mantle that were inferred in this study and from shear-wave splitting observations, respectively. The result is important for understanding the lithospheric dynamics in SE Tibet.

The stress field and kinematics of the crust in Yunnan have also been calculated with GPS observations and Quaternary fault slip rate data (Fig. 7) (e.g., Flesch et al. 2005; Wang et al. 2008). The maximum horizontal stress ($S_H$) revealed in this study is generally consistent with the surface movement of GPS observations (Fig. 7a) (Gan et al. 2007), which show a fan-shaped style in SE Tibet. The present minimum horizontal stress orientations (i.e., $S_h$) is consistent with the maximum extension revealed by GPS and Quaternary fault slip data (Fig. 7b) (Wang et al. 2008). Focal mechanism solutions determined with many small-to-moderate events in separated regions reveal the same pattern of stress field in east Tibet (Xu et al. 1987). These results suggest that the stress field obtained in this study is true and represents the first-order pattern in the crust in Yunnan SE to Tibet.

The fan-shaped pattern of stress field in Yunnan is only part of the large-scale stress pattern in and around the Tibetan plateau or even extending to east China (e.g., Xu et al. 1987). The *P* axis rotates from NW-SE in western Tibet to nearly N-S in northern Tibet and Tianshan, further to NE-SW in eastern Tibet, and finally to E-W and NE-SW in Yunnan of SE Tibet. England and Houseman (1989) calculated the finite strain field in continental deformation and found the stress field in and around the Tibetan Plateau may be explained by a thin viscous sheet model under the Indian-Asian collision. Alternatively, Xu et al. (1987) further proposed the descending Burman slab to the west of the Indochina block as another mechanism for the fan-shaped stress field in Yunnan. But this model will cause the extensional regime in quit a large area in Yunnan, which is inconsistent with the dominantly strike-slip regime revealed by focal mechanism solutions (Fig. 3). Thus, we prefer the model of England and Houseman (1989) for the first-order pattern of stress field in SE Tibet.

However, the local normal regime in NW Yunnan (dashed ellipses in Figs. 5b, 6b) is very annoying. It can hardly be explained by only the England and Houseman's

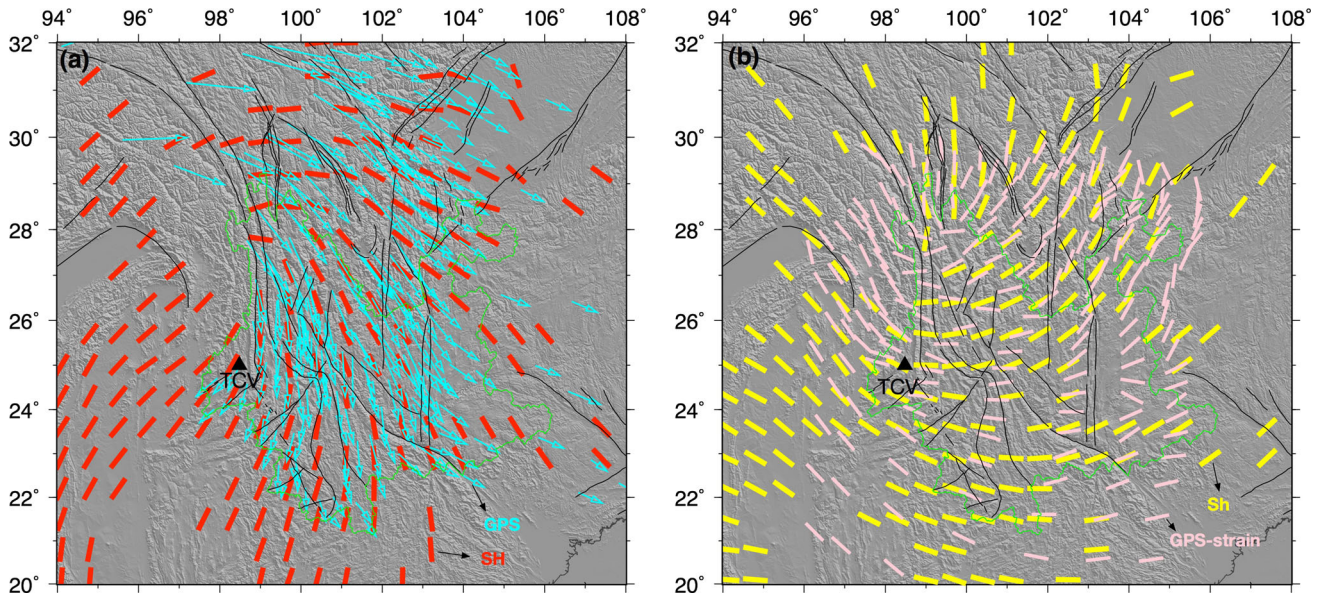


**Fig. 7** **a** Comparison between GPS observations (*blue arrows*) (Gan et al. 2007) and the principal compression ($S_H$; *red bars*) obtained in this study. **b** Comparison between the crustal maximum tensional strain field inverted from the GPS observations (*cyan bars*) (Wang et al. 2008) and the tensional axis ($S_h$; *yellow bars*) obtained in this study. For other labelings, see Fig. 1

(1989) model. Seismic tomography shows important extensive low-velocity zones in the upper mantle under Yunnan which are proposed as back-arc spreading due to the subduction of the Indian or Burman Plate (e.g., Ni et al. 1989; Li et al. 2008; Lei et al. 2009; Wang et al. 2010; Wei et al. 2012; Huang et al. 2015b). There is possible asthenospheric flow from SE Tibet to eastern China (e.g., Li et al. 2008; Lei et al. 2014; Huang et al. 2015b, c) that may probably help the lithosphere of the Indochina and South China blocks above it move southeastward (e.g., Tapponnier et al. 1982, 2001). Such mechanism may induce extensional regional in the whole lithosphere between Tibet (belongs to Eurasian plate) and Yunnan (belongs to Indochina and South China blocks). Another mechanism may arise from the gravity potential and instability in Yunnan. When the Tibetan plateau grows, there is great gravity potential energy at the edge of the high plateau. Thus the change is expected that from topographic gradient-parallel extension at high elevations to topographic gradient-parallel shortening at lower elevations as the collapsing lithosphere encounters resistance from surrounding regions (e.g., Flesch et al. 2005; Wang et al. 2008). The mechanisms are well supported by our results that show dominant N-S horizontal extension (i.e., $S_h$) at elevation greater than 3000 m and gradient-normal $S_h$ at elevation lower than 3000 m (Fig. 8). A fundament difference between the two mechanisms is that the extensional regime is located in the whole lithosphere for the first mechanism while only in the shallow part (e.g., crust) for the second mechanism (e.g., Wang et al. 2008). Therefore, it is necessary to study the stress field in the lithospheric mantle to better explain the tectonics and dynamics in east Tibet.

Whatever the specific mechanism is, both previous and present studies confirm the first-order pattern of the stress/strain field in the crust under Yunnan. The mantle strain field is usually inferred from teleseismic shear-wave (e.g., SKS) splitting observations where the fast polarization directions of the fast S wave is parallel to the maximum strain axes (e.g., Mainprice 2007; Karato et al. 2008). The average delay times of SKS splitting in Yunnan are of the order of 1.0–1.5 s (e.g., Flesch et al. 2005; Lev et al. 2006; Huang et al. 2007, 2011a, 2015a; Sol et al. 2007; Wang et al. 2008, 2013). Contribution of crustal anisotropy inferred from Pms splitting (Sun et al. 2013) and surface wave inversion (Yao et al. 2010) is generally <0.3 s in most Yunnan in spite of some larger delay time to the north of 26°N (Sun et al. 2012). Thus the SKS splitting observations mainly reflect strain field in the upper mantle in Yunnan, in particular to the south of 26°N. Comparison between the crustal stress/strain field and SKS splitting measurements shows that the strain fields in the crust and upper mantle are the same in Yunnan but different in other regions (Fig. 9). The result suggests that the crust and upper mantle under Yunnan are probably coupled and the observed shear-wave splitting can be partly explained by

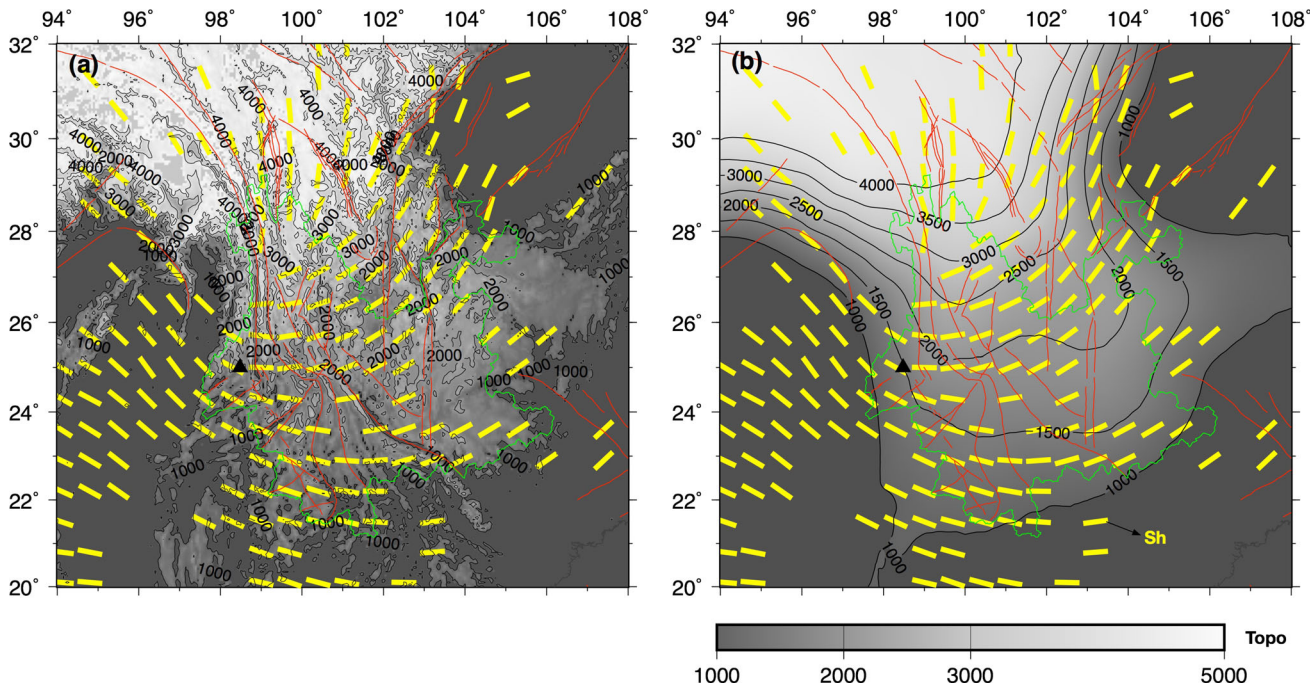


**Fig. 8** **a** Comparison between topography and the horizontal minimum stress (i.e., tensional axis $S_h$; *yellow bars*) obtained in this study. **b** Same as (**a**) but for a smoothed topography. For other labelings, see Fig. 1

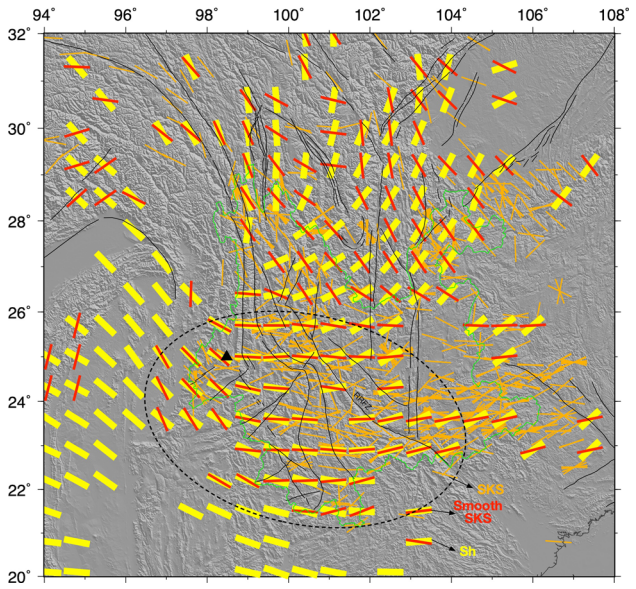


**Fig. 9** Comparison between teleseismic shear-wave (e.g., SKS) splitting observations (*orange* and *red bars*) and the tensional axis ($S_h$; *yellow bars*) obtained in this study. The *orange bars* are the individual shear-wave splitting measurements in this region (e.g., Flesch et al. 2005; Huang et al. 2007, 2011a, 2015a; Lev et al. 2006; Sol et al. 2007; Wang et al. 2008, 2013) while the *red bars* are the smoothed averages in 2° × 2° areas surrounding the grid node

the pure-shear deformation in the lithosphere (e.g., Huang et al. 2015a). Therefore, the model of lateral lithospheric extrusion (e.g., Tapponnier et al. 1982, 2001) or thickening Asian crust (England and Houseman 1989) is potential model for the tectonics and dynamics in Yunnan SE to Tibet while ductile mid-lower crustal flow (e.g., Royden et al. 1997, 2008) does not exist to the south of 26°N in Yunnan.

## 5 Conclusions

We determined the focal mechanism solutions of 239 events ($3.0 \leq M_W \leq 6.0$) with the waveforms recorded by the dense ChinArray stations deployed in Yunnan from August 2011 to December 2013. Then we combined our dataset with 447 focal mechanisms determined in previous studies and inverted the total of 686 focal mechanisms for the first-order pattern of stress field in the crust of Yunnan with a damped linear inversion. Overall, the results indicate dominantly strike-slip environment in Yunnan as both the maximum ($\sigma_1$) and minimum ($\sigma_3$) principal stress axes are sub-horizontal while an extensional regime is found in northwest Yunnan.

We further calculated the horizontal stress orientations and identified the maximum and minimum horizontal compressive stress axes ($S_H$ and $S_h$, respectively) in the crust. The horizontal stress axes change abruptly near ~26°N. To the north, $S_H$ aligns NW-SE to nearly E-W while $S_h$ aligns nearly N-S. In contrast, to the south, both $S_H$ and $S_h$ rotate laterally and show dominantly fan-shaped patterns. $S_H$ rotates from NE-SW to the west of Tengchong volcano gradually to nearly N-S in west Yunnan, and further to NW-SE in the South China block in the east. Similarly, $S_h$ rotates from NW-SE in the west to nearly E-W in the middle, and further to NE-SW in the east. The $S_h$ axis (consistent with maximum horizontal strain) in the crust is consistent with that inverted from GPS observations, whereas the maximum strain is normal to the GPS observations. The maximum strain is also normal to the gradients of the topography, suggesting the stress field in the crust mainly arises from the gravity potential and instability near the edge of the high plateau. The crustal strain field is consistent with the upper mantle strain field inferred from shear-wave splitting observations in Yunnan but not in other regions. Thus the crust and upper mantle in Yunnan are coupled and suffering vertically coherent pure-shear deformation in the lithosphere, which partly explained the observed shear-wave splitting.

**Acknowledgments** The waveform data was provided by China Seismic Array Data Management Center at Institute of Geophysics, China Earthquake Administration. Two anonymous reviewers provided constructive comments and suggestions that greatly improved the manuscript. This work was supported by the National Natural Science Foundations of China (No. 41204040) and China National Special Fund for Earthquake Scientific Research in Public Interest (Nos. 201008001, 201308011). Most figures were made using GMT (Wessel et al. 2013).



## References

Aki K, Richards PG (2002) Quantitative seismology, 2nd edn. University Science Books, California

Cui X, Xie F, Zhang H (2006) Recent tectonic stress field zoning in Sichuan Yunnan region and it dynamic interest. Acta Seismol Sin 28:451–461 **(in Chinese with English abstract)**

England P, Houseman G (1989) Extension during continental convergence: with application to the Tibetan Plateau. J Geophys Res 94:17561–17579

Flesch L, Holt W, Silver P, Stephenson M, Wang C, Chan W (2005) Constraining the extent of crust–mantle coupling in central Asia using GPS, geologic, and shear wave splitting data. Earth Planet Sci Lett 238:248–268

Gan W, Zhang P, Shen ZK, Niu Z, Wang M, Wan Y, Zhou D, Cheng J (2007) Present-day crustal motion within the Tibetan Plateau inferred from GPS measurements. J Geophys Res 112:B08416

Gephart JW, Forsyth DW (1984) An improved method for determining the regional stress tensor using earthquake focal mechanism

data: application to the San Fernando earthquake sequence. J Geophys Res 89:B119305
Hardebeck J, Hauksson E (2001) Crustal stress field in southern California and its implications for fault mechanics. J Geophys Res 106:21859–21882
Hardebeck JL, Michael AJ (2006) Damped regional-scale stress inversions: methodology and examples for southern California and the Coalinga aftershock sequence. J Geophys Res 111(11):1–11
Huang Z, Wang L, Xu M, Liu J, Mi N, Liu S (2007) Shear wave splitting across the Ailao Shan-Red River fault zone, SW China. Geophys Res Lett 34:L20301
Huang Z, Wang L, Zhao D, Mi N, Xu M (2011a) Seismic anisotropy and mantle dynamics beneath China. Earth Planet Sci Lett 306:105–117
Huang Z, Zhao D, Wang L (2011b) Stress field in the 2008 Iwate-Miyagi earthquake (M7.2) area. Geochem Geophys Geosyst 12:Q06006
Huang Z, Wang L, Xu M, Ding Z, Wu Y, Wang P, Mi N, Yu D, Li H (2015a) Teleseismic shear-wave splitting in SE Tibet: insight into complex crust and upper-mantle deformation. Earth Planet Sci Lett 432:354–362
Huang Z, Wang P, Xu M, Wang L, Ding Z, Wu Y, Xu M, Mi N, Yu D, Li H (2015b) Mantle structure and dynamics beneath SE Tibet revealed by new seismic images. Earth Planet Sci Lett 411:100–111
Huang Z, Zhao D, Wang L (2015c) P wave tomography and anisotropy beneath Southeast Asia: insight into mantle dynamics. J Geophys Res 120:5154–5174
Karato S, Jung H, Katayama I, Skemer P (2008) Geodynamic significance of seismic anisotropy of the upper mantle: new insights from laboratory studies. Annu Rev Earth Planet Sci 36:59–95
Lei JS, Zhao DP, Su YJ (2009) Insight into the origin of the Tengchong intraplate volcano and seismotectonics in southwest China from local and teleseismic data. J Geophys Res 114:B05302
Lei JS, Li Y, Xie FR, Teng JW, Zhang GW, Sun CQ, Zha XH (2014) Pn anisotropic tomography and dynamics under eastern Tibetan plateau. J Geophys Res 119:2174–2198
Lev E, Long MD, Van der Hilst R (2006) Seismic anisotropy in Eastern Tibet from shear wave splitting reveals changes in lithospheric deformation. Earth Planet Sci Lett 251:293–304
Li C, Van der Hilst RD, Meltzer AS (2008) Subduction of the Indian lithosphere beneath the Tibetan Plateau and Burma. Earth Planet Sci Lett 274:157–168
Lund B, Townend J (2007) Calculating horizontal stress orientations with full or partial knowledge of the tectonic stress tensor. Geophys J Int 170:1328–1335
Luo J, Zhao C, Zhou L (2014) Characteristics of focal mechanisms and stress field of the Chuan-Dian rhombic block and it adjacent regions. Seismol Geol 36:405–421. (**in Chinese with English abstract**)
Ma W, Xu X, Cao Z, Yu G, Li H, Xu C (2008) Classification of focal mechanism solutions and characteristics of latest crustal deformation of Sichuan-Yunnan region and it adjacency. Seismol Geol 30:926–934 **(in Chinese with English abstract)**
Mainprice D (2007) Seismic anisotropy of the deep Earth from a mineral and rock physics perspective. Treatise Geophys 2:437–491
Martinez-Garzon P, Kwiatek G, Ickrath M, Bohnhoff M (2014) MSATSI: a MATLAB package for stress inversion combining solid classic methodology, a new simplified user-handling, and a visualization tool. Seismol Res Lett 85(4):896–904
Michael AJ (1987) Use of focal mechanisms to determine stress: a control study. J Geophys Res 92:B1357
Ni JF, Guzmanspeziale M, Bevis M, Holt WE, Wallace TC, Seager WR (1989) Accretionary tectonics of Burma and the 3-dimensional geometry for the Burma subduction zone. Geology 17:68–71
Qian X, Qin J, Liu L (2011) Study on recent tectonic stress field in Yunnan region. Seismol Geol 33:91–106 **(in Chinese with English abstract)**
Ren J (1999) Tectonic map of China and adjacent regions 1: 5,000,000. Geological Publishing House, Beijing
Royden LH, Burchfiel BC, King RW, Wang E, Chen Z, Shen F, Liu Y (1997) Surface deformation and lower crustal flow in eastern Tibet. Science 27:788–790
Royden LH, Burchfiel BC, Van der Hilst RD (2008) The geological evolution of the Tibetan Plateau. Science 321:1054–1058
Schimitt DR, Currie CA, Zhang L (2012) Crustal stress determination from boreholes and rock cores: fundamental principles. Tectonophysics 580:1–26
Scholz CH (2002) The mechanics of earthquakes and faulting, 1st edn. Cambridge University Press, Cambridge
Sol S, Meltzer A, Bürgmann R, Van der Hilst RD, King R, Chen Z, Koons PO, Lev E, Liu YP, Zeitler PK, Zhang X, Zhang J, Zurek B (2007) Geodynamics of the southeastern Tibetan Plateau from seismic anisotropy and geodesy. Geology 35:563–566
Sun Y, Niu F, Liu H, Chen Y, Liu J (2012) Crustal structure and deformation of the SE Tibetan plateau revealed by receiver function data. Earth Planet Sci Lett 349–350:186–197
Sun C, Lei J, Li C, Zhang G, Zha X, Li F (2013) Crustal anisotropy beneath the Yunnan region and dynamic implications. Chin J Geophys 12:4095–4105 **(in Chinese with English abstract)**
Tapponnier P, Peltzer G, Dain AY, Le Armijo R, Jussieu P, Cobbold P (1982) Propagating extrusion tectonics in Asia: new insights from simple experiments with plasticine. Geology 10:611–616
Tapponnier P, Zhiqin X, Roger F, Meyer B, Arnaud N, Wittlinger G, Jingsui Y (2001) Oblique stepwise rise and growth of the Tibet plateau. Science 294:1671–1677
Wan Y (2010) Contemporary tectonic stress field in China. Earthq Sci 23:377–386
Wang CY, Chan WW, Mooney WD (2003) Three-dimensional velocity structure of crust and upper mantle in southwestern China and its tectonic implications. J Geophys Res 108:B92442
Wang CY, Flesch LM, Silver PG, Chang L, Chan W (2008) Evidence for mechanically coupled lithosphere in central Asia and resulting implications. Geology 36:363–366
Wang CY, Zhu LP, Lou H, Huang BS, Yao ZX, Lou XH (2010) Crustal thickness and Poisson's ratios in the eastern Tibetan Plateau and their tectonic implications. J Geophys Res 115:B11301
Wang CY, Flesch LM, Chang L, Zheng T (2013) Evidence of active mantle flow beneath South China. Geophys Res Lett 40:5137–5141
Wei W, Xu J, Zhao D, Shi Y (2012) East Asia mantle tomography: new insight into plate subduction and intraplate volcanism. J Asian Earth Sci 60:88–103
Wessel P, Smith WHF, Scharroo R, Luis J, Wobbe F (2013) Generic mapping tools: improved version released. EOS Trans AGU 94:409–410
Xie F, Zhu J, Liang H, Liu G (1993) Tectonic stress in southeast China. Acta Seismol Sin 15:407–417 **(in Chinese with English abstract)**
Xu Z, Wang S, Huang Y, Gao A, Jin X, Chang X (1987) Directions of mean stress axes in southwestern China deduced from micro-earthquake data. Acta Geophys Sin 30:476–486 **(in Chinese with English abstract)**
Xu Y, Herrmann RB, Koper KD (2010) Source parameters of regional small-to-moderate earthquakes in the Yunnan-Sichuan region of China. Bull Seismol Soc Am 100(5B):2518–2531

Yao H, van der Hilst RD, Montagner JP (2010) Heterogeneity and anisotropy of the lithosphere of SE Tibet from surface wave array tomography. J Geophys Res 115:B12307

Zhao L, Helmberger D (1994) Source estimation from broadband regional seismograms. Bull Seismol Soc Am 84(1):91–104

Zhao L, Luo Y, Liu T, Luo YJ (2013) Earthquake focal mechanisms in Yunnan and their inference on the regional stress field. Bull Seismol Soc Am 103(4):2498–2507

Zhu L, Ben-Zion Y (2013) Parametrization of general seismic potency and moment tensors for source inversion of seismic waveform data. Geophys J Int 194:839–843

Zhu L, Helmberger DV (1996) Advancement in source estimation techniques using broadband regional seismograms. Bull Seismol Soc Am 86(5):1634–1641

Zhu L, Rivera LA (2002) A note on the dynamic and static displacements from a point source in multilayered media. Geophys J Int 148:619–627